J. Fluid. Mech. (1982), *vol.* 124, *pp.* 283–306
Printed in Great Britain

Steep standing waves at a fluid interface

By JAMES W. ROTTMAN

Department of Applied Mathematics and Theoretical Physics, University of Cambridge, Silver Street, Cambridge CB3 9EW

(Received 3 November 1981 and in revised form 23 June 1982)

An algorithm is formulated for computing perturbation-series solutions for standing waves on the interface between two semi-infinite fluids of different but uniform densities. Using a computer, the series solutions are computed to fifth order for a general value of r, the ratio of the density of the upper fluid to that of the lower fluid ($0 \leqslant r \leqslant 1$), and to 21st order for five specific values of this ratio: $r = 0$, 10^{-3}, 0·1, 0·5, 1·0. The series for the period, the energy, and the interface profile of the waves are summed using Padé approximants. The maximum wave height for each of the above five density ratios is estimated from the locations of the poles of the Padé approximants for the wave period and the wave energy. At maximum height the interface appears to be vertical at a point on the interface that is very near the crest for $r = 10^{-3}$ and approaches the midpoint between the crest and the trough as r approaches 1·0.

1. Introduction

Two-dimensional standing waves at a fluid interface are fluid motions, bounded by an interface between two fluids of different but uniform densities, that are periodic in both space and time and are symmetric about some plane that is perpendicular to the undisturbed interface. Because standing waves cannot be reduced to steady motion by a change of coordinate system, the mathematical determination of standing waves is a more difficult problem than that of progressive waves of permanent form. There is no mathematical proof of the existence of standing waves that satisfy the exact boundary conditions, but several approximate small-amplitude solutions have been determined.

Most of the previous work is concerned with free-surface standing waves, a special case of interfacial standing waves in which the density of the upper fluid is zero. Rayleigh (1915) was the first to investigate the nonlinear behaviour of free-surface standing waves. He developed perturbation-expansion procedures, valid for small amplitudes, and computed the expansions to third order in the expansion parameter for the case of a fluid of infinite depth. Much later, Penney & Price (1952), essentially using Rayleigh's method, computed the expansion to fifth order. Using a different expansion procedure, Tadjbaksh & Keller (1960) computed expansions to third order for the case of finite depth. Using a Lagrangian coordinate system instead of the Eulerian coordinates of the previously mentioned investigations, Sekerzh-Zenkovich (1947, 1951) and Chabert D'Hieres (1960) developed alternative perturbation-expansion procedures and computed expansions to third order for both infinite and finite depth. More recently, Schwartz & Whitney (1977, 1981), using the conformal-mapping methods described by Whitney (1971), formulated a simpler perturbation-expansion procedure, which they used to compute a 25th-order expansion with the aid of a computer for a fluid of infinite depth.

For comparison with interfacial waves, we describe here some properties of nonlinear free-surface standing waves. The calculations discussed above show that the maximum elevation of the free surface from its mean level exceeds the maximum depression. Also, the period of the waves increases with increasing amplitude for depth-to-wavelength ratios greater than 0·17, and decreases with increasing amplitude for depth-to-wavelength ratios less than 0·17. This behaviour has been verified experimentally by Fultz (1962). The fifth-order calculations of Penney & Price show that the free surface is never flat.

Penney & Price (1952) proposed that the free-surface standing wave of maximum amplitude, when at its maximum height, has a downward acceleration at the crest equal to g. Their proposal is based on the assertion, established rigorously by Schwartz & Whitney (1981), that the downward acceleration of the crest cannot exceed g. Using this criterion, Penney & Price estimated that the maximum wave-height-to-wavelength ratio is 0·218. With the further assumption that the pressure may be expanded in a Taylor series about the crest, they concluded that the wave of maximum amplitude would crest in a corner with an enclosed angle of 90°. The experiments of Taylor (1953) and Edge & Walters (1964) show that the wave of maximum amplitude has a nearly 90° corner at the crest, but the wave height (only measured by Taylor) is about 10 % greater than predicted by Penney & Price. Taylor (1953) disputed Penney & Price's argument for the 90° crest angle because the argument is independent of the mode of formation of the crest. The high-order perturbation expansion of Schwartz & Whitney (1981) also suggests, but not conclusively, that the wave of maximum amplitude has a 90° corner at the crest, and predicts that the maximum wave-height-to-wavelength ratio is between 0·204 and 0·213. Schwartz & Whitney (1981) also find the argument for the 90° crest corner unconvincing because the pressure may not be a regular function in the neighbourhood of a sharp crest. Saffman & Yuen (1979), having recently completed some time-dependent numerical calculations of standing waves, claim that their results do not support the argument for a 90° crest corner.

Interfacial standing waves, which are of interest in many physical situations, have received less attention. For fluids of infinite depth Hunt (1961), using basically Penney & Price's method, computed a fourth-order perturbation expansion, and Sekerzh-Zenkovich (1961), using an appropriately modified version of his earlier free-surface Lagrangian formulation, computed a third-order expansion. Thorpe (1968) extended Hunt's analysis to include the effects of finite fluid depth. These calculations show that the presence of the upper fluid reduces the influence of higher harmonics in the solution, making the interface profile more sinusoidal in shape than a free-surface profile of equivalent amplitude. Also, the presence of the upper fluid increases the period of the oscillations. For ratios of the density of the upper fluid to that of the lower fluid between 0·97 and 1·0, Thorpe (1968) has checked experimentally some of the theoretical predictions of the properties of interfacial standing waves. He found good agreement between theory and experiment for the shape of the interface and the period of the waves at small wave amplitudes.

In none of the previously mentioned theoretical work is the shape or amplitude of the highest interfacial standing wave estimated. Thorpe (1968) observed experimentally, for the density ratios mentioned above, that interfacial standing waves become unstable at a wave-height-to-wavelength ratio of about 0·13. The instability begins as a single vortex at the node of the waves, and thereafter the motion quickly becomes three-dimensional. Thorpe suggests that the observed instability is a shear instability.

In the present work we formulate an algorithm for computing high-order perturbation-series solutions for interfacial standing waves. We compute the series to fifth order for a general value of r, the ratio of the density of the upper fluid to that in the lower fluid, and to 21st order for five specific values of this ratio, $r = 0{\cdot}0$, 10^{-3}, $0{\cdot}1$, $0{\cdot}5$, $1{\cdot}0$. We use Padé approximants to sum the series for the wave period, the wave energy, and the wave profile. The positions of the poles of the Padé approximants for the wave period and wave energy are used to estimate the amplitude of the highest wave for the five density ratios given above, although we do not have a sufficient number of terms to give conclusive answers. Our results suggest, in agreement with Schwartz & Whitney (1981), that the highest free-surface standing wave has a wave-height-to-wavelength ratio of about $0{\cdot}21$, which occurs when the fluid acceleration at the crest equals g and the enclosed angle at the crest is 90°. For Boussinesq ($r = 1$) waves, our results indicate that the maximum wave-height-to-wavelength ratio is about $0{\cdot}35$. Inspection of Boussinesq wave profiles leads us to conclude that the wave of maximum amplitude has a vertical slope at its node. We can detect no significant difference between free-surface ($r = 0$) and air–water ($r = 10^{-3}$) waves. We find that $r = 0{\cdot}1$ waves have a maximum amplitude much larger than Boussinesq waves, and $r = 0{\cdot}5$ waves have a maximum amplitude between those of free-surface and Boussinesq waves. We conclude from our computed wave profiles that the wave of maximum height, for given $r > 0$, has a vertical slope at some point along the interface, and that this point moves from very near the crest to midway between the crest and the trough as the density ratio increases from very near zero to one.

The mathematical formulation of the problem is discussed in §2. A perturbation-expansion procedure, similar to that used by Hunt (1961), and a solution algorithm are described in §3. The results are presented and discussed in §4, and some concluding remarks are offered in §5.

2. Formulation of the problem

We consider the motion under the influence of gravity of symmetric two-dimensional standing waves on the interface between two homogeneous semi-infinite fluids of different densities. Both fluids are assumed to be inviscid and incompressible, and the motion in either fluid is assumed to be irrotational.

In a reference frame in which the fluid at infinity is at rest, we define a rectangular coordinate system such that the x-axis is directed parallel to the undisturbed interface and the y-axis is directed perpendicular to the undisturbed interface and opposite to the direction of gravity. We describe the interface profile by the relation $y = \eta(t, x)$, where t represents time, and position the coordinate system such that the value of η averaged over one wavelength of the motion at any fixed time is zero. All quantities associated with the lower fluid will be denoted by a subscript 1 and all quantities associated with the upper fluid will be denoted by a subscript 2. A schematic diagram of one wavelength of the motion is shown in figure 1.

Because both fluids are incompressible and the motion in each fluid is irrotational, we can define the velocity potentials ϕ_1 and ϕ_2 such that

$$u_1 = \frac{\partial \phi_1}{\partial x}, \quad u_2 = \frac{\partial \phi_2}{\partial x}, \tag{2.1a, b}$$

$$v_1 = \frac{\partial \phi_1}{\partial y}, \quad v_2 = \frac{\partial \phi_2}{\partial y}, \tag{2.2a, b}$$

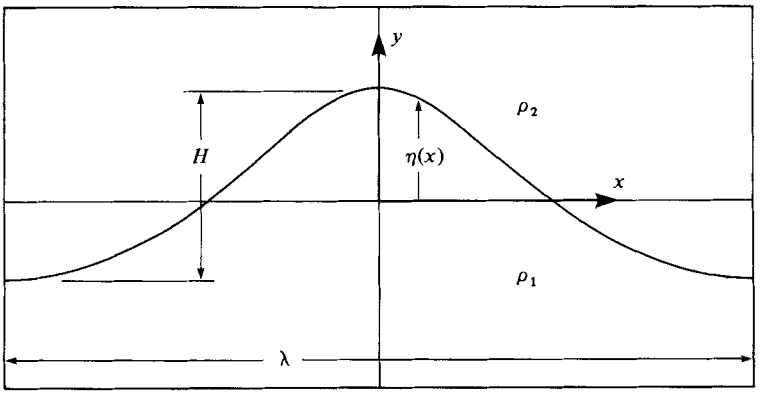

FIGURE 1. A schematic representation of interfacial standing waves, illustrating the coordinate system and nomenclature used in the text.

$$\nabla^2\phi_1 = 0, \quad \nabla^2\phi_2 = 0, \tag{2.3a, b}$$

in which u is the horizontal component and v the vertical component of the fluid velocity. The problem is to determine the shape $y = \eta(t, x)$ of the interface profile at all times, the two functions ϕ_1 and ϕ_2 that satisfy (2.3), and the period T of the motion, such that for specified wave amplitude the motion is periodic in space, with specified wavelength λ, periodic in time, and such that the following boundary conditions are satisfied:

$$\phi_1 \to 0 \quad \text{as} \quad y \to -\infty, \tag{2.4a}$$

$$\phi_2 \to 0 \quad \text{as} \quad y \to +\infty, \tag{2.4b}$$

$$\frac{\partial\eta}{\partial t} + \frac{\partial\phi_1}{\partial x}\frac{\partial\eta}{\partial x} = \frac{\partial\phi_1}{\partial y} \quad \text{on} \quad y = \eta(t, x), \tag{2.5a}$$

$$\frac{\partial\eta}{\partial t} + \frac{\partial\phi_2}{\partial x}\frac{\partial\eta}{\partial x} = \frac{\partial\phi_2}{\partial y} \quad \text{on} \quad y = \eta(t, x), \tag{2.5b}$$

$$p_1 = p_2 \quad \text{on} \quad y = \eta(t, x), \tag{2.6}$$

$$\frac{\partial\phi_1}{\partial x} = \frac{\partial\phi_2}{\partial x} = 0 \quad \text{at} \quad x = 0, \tag{2.7}$$

where p represents the pressure. The boundary condition (2.4) requires the motion to vanish far from the interface, (2.5) states that the normal component of the fluid velocity on the interface must equal the normal component of the interface velocity, (2.6) asserts that the pressure must be continuous across the interface, and (2.7) fixes the phase of the waves, making $x = 0$ a plane of symmetry. We define the wave amplitude H as the vertical distance from the crest to the trough at $t = 0$.

The pressure may be eliminated from the problem by use of Bernoulli's equation, which relates the pressure to the velocity potential by

$$\frac{p_1}{\rho_1} + \frac{\partial\phi_1}{\partial t} + \tfrac{1}{2}(\nabla\phi_1)^2 + gy = B_1(t), \tag{2.8}$$

$$\frac{p_2}{\rho_2} + \frac{\partial\phi_2}{\partial t} + \tfrac{1}{2}(\nabla\phi_2)^2 + gy = B_2(t), \tag{2.9}$$

where ρ is the density, g is the acceleration due to gravity, and $B_1(t)$ and $B_2(t)$ are functions of t only. Subtracting (2.9) from (2.8), we write (2.6) as

$$\frac{\partial \phi_1}{\partial t} - r\frac{\partial \phi_2}{\partial t} + \tfrac{1}{2}(\nabla\phi_1)^2 - r\tfrac{1}{2}(\nabla\phi_2)^2 + (1-r)g\eta = B(t), \tag{2.10}$$

where

$$B(t) = B_1(t) - rB_2(t), \tag{2.11}$$

$$r = \frac{\rho_2}{\rho_1}. \tag{2.12}$$

We may obtain an expression for $B(t)$ in (2.10) in terms of the dependent variables of the problem. Defining the modified pressure P as the deviation of the pressure from its hydrostatic value, we infer from (2.8) and (2.9) that far from the interface

$$\frac{P_1}{\rho_1} \to B_1(t) \quad \text{as} \quad y \to -\infty, \tag{2.13}$$

$$\frac{P_2}{\rho_2} \to B_2(t) \quad \text{as} \quad y \to +\infty. \tag{2.14}$$

Thus $B_1(t)$ and $B_2(t)$ are proportional to the component of the pressure in each of the two fluids that is spatially uniform and time-dependent. For standing waves, the centre of mass of the two-fluid system oscillates vertically with twice the frequency of the waves. Equating the net total external force per unit horizontal area to the acceleration of the centre of mass per unit horizontal area, we obtain the expression

$$P_1(y=-\infty) - P_2(y=+\infty) = \frac{1}{\lambda}\frac{d^2}{dt^2}\left(\int_0^\lambda \int_{-\infty}^{\eta} \rho_1 y\, dy\, dx + \int_0^\lambda \int_{\eta}^{\infty} \rho_2 y\, dy\, dx\right), \tag{2.15}$$

and thus

$$B(t) = \tfrac{1}{2}(1-r)\frac{d^2\overline{\eta^2}}{dt^2}, \tag{2.16}$$

where the overbar denotes horizontal average over one wavelength.

To determine the pressure in each of the two fluids, an additional boundary condition that specifies the pressure far from the interface in one of the two fluids is required. A common laboratory situation would have a stationary free surface far above the interface, with the associated boundary condition that the pressure in the upper fluid far from the interface must vanish. In the present work, we do not compute the absolute pressure, and therefore need not specify this additional boundary condition.

One of the main difficulties with all water-wave problems is that the nonlinear boundary conditions (2.5) and (2.10) are applied at the unknown position of the interface. For free-surface progressive waves, this difficulty is eliminated by making the space coordinates the dependent variables and the stream function and the velocity potential the independent variables; the free surface is then known, since it must be a streamline. For free-surface standing waves, Schwartz & Whitney (1981) showed that this difficulty can be reduced by computing a time-dependent conformal mapping that maps the fluid region onto a time-independent region, and thus maps the free surface onto a known line. However, for interfacial waves, these methods are of no advantage. Holyer (1979) discusses this problem for interfacial progressive waves. For interfacial standing waves, no conformal mapping can map both upper and lower fluids to a fixed region such that adjacent points of the two fluids on opposite sides of the interface are mapped to adjacent points in the new region. We

follow Holyer (1979), and expand the boundary conditions (2.5) and (2.10) in Taylor series about the undisturbed interface $y = 0$. Thus (2.5) and (2.10) become

$$\frac{\partial \eta}{\partial t} - \frac{\partial \phi_1}{\partial y} = -\frac{\partial \eta}{\partial x}\frac{\partial \phi_1}{\partial x} + \sum_{j=1}^{\infty}\left[\frac{\eta^j}{j!}\left(\frac{\partial^{j+1}\phi_1}{\partial y^{j+1}} - \frac{\partial \eta}{\partial x}\frac{\partial^{j+1}\phi_1}{\partial x \partial y^j}\right)\right], \tag{2.17a}$$

$$\frac{\partial \eta}{\partial t} - \frac{\partial \phi_2}{\partial y} = -\frac{\partial \eta}{\partial x}\frac{\partial \phi_2}{\partial x} + \sum_{j=1}^{\infty}\left[\frac{\eta^j}{j!}\left(\frac{\partial^{j+1}\phi_2}{\partial y^{j+1}} - \frac{\partial \eta}{\partial x}\frac{\partial^{j+1}\phi_2}{\partial x \partial y^j}\right)\right], \tag{2.17b}$$

$$\frac{\partial \phi_1}{\partial t} - r\frac{\partial \phi_2}{\partial t} + (1-r)g\eta = B - \tfrac{1}{2}(\nabla\phi_1)^2 + \tfrac{1}{2}r(\nabla\phi_2)^2 + \sum_{j=1}^{\infty}\left\{\frac{\eta^j}{j!}\frac{\partial^j}{\partial y^j}\left[-\frac{\partial \phi_1}{\partial t} + r\frac{\partial \phi_2}{\partial t} - \tfrac{1}{2}(\nabla\phi_1)^2 + \tfrac{1}{2}r(\nabla\phi_2)^2\right]\right\}. \tag{2.18}$$

Our working equations are (2.3) with the boundary conditions (2.4), (2.7), (2.17) and (2.18). To make these equations non-dimensional, we choose k^{-1}, where $k = 2\pi/\lambda$ is the wavenumber, as our reference length, and ω^{-1}, where $\omega = 2\pi/T$ is the angular frequency, as our reference time. The dimensionless variables (denoted by a tilde) are

$$\tilde{x} = kx, \quad \tilde{y} = ky, \quad \tilde{t} = \omega t, \tag{2.19a, b, c}$$

$$\tilde{\phi}_1 = \frac{k^2}{\omega}\phi_1, \quad \tilde{\phi}_2 = \frac{k^2}{\omega}\phi_2, \quad \tilde{\eta} = k\eta, \tag{2.20a, b, c}$$

and the resulting non-dimensional parameter is

$$S \equiv \frac{g(1-r)\,k}{\omega^2}. \tag{2.21}$$

The substitution of the non-dimensional variables into the governing equations and the subsequent dropping of the tildes leaves all the equations unchanged except that $(1-r)g$ in (2.18) is replaced by S. This parameter is proportional to the square of the period of the waves; it is also simply the non-dimensional reduced acceleration due to gravity.

3. Perturbation solution

We seek a perturbation solution to the problem formulated in §2. Therefore, we expand the dependent variables in power series in terms of a perturbation parameter ϵ:

$$\eta(t, x) = \sum_{l=1}^{\infty} \eta^{(l)}\epsilon^l, \tag{3.1}$$

$$\phi_1(t, x, y) = \sum_{l=1}^{\infty} \phi_1^{(l)}\epsilon^l, \tag{3.2}$$

$$\phi_2(t, x, y) = \sum_{l=1}^{\infty} \phi_2^{(l)}\epsilon^l, \tag{3.3}$$

$$B(t) = \sum_{l=1}^{\infty} B^{(l)}\epsilon^l, \tag{3.4}$$

$$S = \sum_{l=0}^{\infty} S^{(l)}\epsilon^l. \tag{3.5}$$

ϵ is defined to be half the vertical distance from the crest to the trough at the time $t = 0$:

$$\epsilon = \tfrac{1}{2}H = \tfrac{1}{2}[\eta(0, 0) - \eta(0, \pi)]. \tag{3.6}$$

Substituting (3.1)–(3.5) into (2.3), (2.4), (2.7), (2.17), (2.18) and (3.6), and equating coefficients of ϵ^l (for $l = 1, 2, 3, \ldots$) to zero in each equation, we obtain the following:

$$\nabla^2\phi_1^{(l)} = 0, \quad \nabla^2\phi_2^{(l)} = 0, \tag{3.7a, b}$$

$$\phi_1^{(l)} \to 0 \quad \text{as} \quad y \to -\infty, \quad \phi_2^{(l)} \to 0 \quad \text{as} \quad y \to +\infty, \tag{3.8a, b}$$

$$\frac{\partial\eta^{(l)}}{\partial t} - \frac{\partial\phi_1^{(l)}}{\partial y} = f^{(l)} \quad \text{on} \quad y = 0, \tag{3.9a}$$

$$\frac{\partial\eta^{(l)}}{\partial t} - \frac{\partial\phi_2^{(l)}}{\partial y} = g^{(l)} \quad \text{on} \quad y = 0, \tag{3.9b}$$

$$\frac{\partial\phi_1^{(l)}}{\partial t} - r\frac{\partial\phi_2^{(l)}}{\partial t} + S^{(0)}\eta^{(l)} = B^{(l)} + h^{(l)} - S^{(l-1)}\eta^{(1)}(1-\delta_{l,1}) \quad \text{on} \quad y = 0, \tag{3.10}$$

$$\frac{\partial\phi_1^{(l)}}{\partial x} = \frac{\partial\phi_2^{(l)}}{\partial x} = 0 \quad \text{at} \quad x = 0, \tag{3.11}$$

$$\eta^{(l)}(0,0) - \eta^{(l)}(0,\pi) = \delta_{l,1}, \tag{3.12}$$

where δ_{ij} is the Kronecker delta, and

$$f^{(l)} = -\sum_{k=1}^{l-1} \frac{\partial\eta^{(k)}}{\partial x}\frac{\partial\phi_1^{(l-k)}}{\partial x} + \sum_{j=1}^{l-1}\sum_{k=1}^{l-j} E_j^{(j+k-1)} F_j^{(l-j-k+1)}, \tag{3.13}$$

$$g^{(l)} = -\sum_{k=1}^{l-1} \frac{\partial\eta^{(k)}}{\partial x}\frac{\partial\phi_2^{(l-k)}}{\partial x} + \sum_{j=1}^{l-1}\sum_{k=1}^{l-j} E_j^{(j+k-1)} G_j^{(l-j-k+1)}, \tag{3.14}$$

$$\begin{aligned} h^{(l)} = &-\tfrac{1}{2}\sum_{k=1}^{l-1}\left[\frac{\partial\phi_1^{(k)}}{\partial x}\frac{\partial\phi_1^{(l-k)}}{\partial x} + \frac{\partial\phi_1^{(k)}}{\partial y}\frac{\partial\phi_1^{(l-k)}}{\partial y}\right] \\ &+\tfrac{1}{2}r\sum_{k=1}^{l-1}\left[\frac{\partial\phi_2^{(k)}}{\partial x}\frac{\partial\phi_2^{(l-k)}}{\partial x} + \frac{\partial\phi_2^{(k)}}{\partial y}\frac{\partial\phi_2^{(l-k)}}{\partial y}\right] \\ &+\sum_{j=1}^{l-1}\sum_{k=1}^{l-j} E_j^{(j+k-1)} H_j^{(l-j-k+1)} - \sum_{k=1}^{l-2} S^{(k)}\eta^{(l-k)}, \end{aligned} \tag{3.15}$$

$$E_1^{(l)} = \eta^{(l)}, \quad E_j^{(l)} = \frac{1}{j}\sum_{k=1}^{l-j+1} \eta^{(k)} E_{j-1}^{(l-k)} \quad (j = 2, 3, \ldots, l-1), \tag{3.16}$$

$$F_j^{(l)} = \frac{\partial^{j+1}\phi_1^{(l)}}{\partial y^{j+1}} - \sum_{k=1}^{l-1} \frac{\partial\eta^{(k)}}{\partial x}\frac{\partial^{j+1}\phi_1^{(l-k)}}{\partial x\partial y^j} \quad (j = 1, 2, \ldots, l-1), \tag{3.17}$$

$$G_j^{(l)} = \frac{\partial^{j+1}\phi_2^{(l)}}{\partial y^{j+1}} - \sum_{k=1}^{l-1} \frac{\partial\eta^{(k)}}{\partial x}\frac{\partial^{j+1}\phi_2^{(l-k)}}{\partial x\partial y^j} \quad (j = 1, 2, \ldots, l-1), \tag{3.18}$$

$$H_j^{(l)} = -\frac{\partial^{j+1}\phi_1^{(l)}}{\partial t\partial y^j} + r\frac{\partial^{j+1}\phi_2^{(l)}}{\partial t\partial y^j} \quad (j = 1, 2, \ldots, l-1), \tag{3.19}$$

where the sums are zero if the upper bound of the index is less than the lower bound.

The functions $f^{(l)}$, $g^{(l)}$ and $h^{(l)}$ are zero for $l = 1$, and are nonlinear combinations of solutions to (3.7)–(3.12) of order less than l for $l > 1$. Thus (3.7)–(3.12) are linear in terms of $\eta^{(l)}$, $\phi_1^{(l)}$, $\phi_2^{(l)}$, $B^{(l)}$, $S^{(l-1)}$, and may be solved successively for $l = 1, 2, \ldots$.

For any order l, (3.7), with boundary conditions (3.8) and (3.11), have the particular solutions

$$\eta_{\mu,\nu} = \cos(\mu t)\cos(\nu x), \tag{3.20}$$

$$\phi_{1\mu,\nu} = \sin(\mu t)\cos(\nu x)\, e^{\nu y}, \tag{3.21}$$

$$\phi_{2\mu,\nu} = \sin(\mu t)\cos(\nu x)\, e^{-\nu y}, \tag{3.22}$$

with $\mu = 0, 1, 2, \ldots$ and $\nu = 1, 2, 3, \ldots$. These solutions have the required periodicity in time and space. The complete solution is determined by choosing the linear combinations of each of (3.20)–(3.22) that satisfy the boundary conditions (3.9) and (3.10), and (3.12).

For $l = 1$, the general periodic solution to (3.7)–(3.12) is

$$\eta^{(1)} = \sum_{m=1}^{\infty} a_m \eta_{m,m^2}, \tag{3.23}$$

$$\phi_1^{(1)} = -\sum_{m=1}^{\infty} m^{-1} a_m \phi_{1m,m^2}, \tag{3.24}$$

$$\phi_2^{(1)} = \sum_{m=1}^{\infty} m^{-1} a_m \phi_{2m,m^2}, \tag{3.25}$$

$$B^{(1)} = 0, \tag{3.26}$$

$$S^{(0)} = 1 + r, \tag{3.27}$$

with the constants a_m subject to the conditions

$$\sum_{n=1}^{\infty} a_{2n-1} = 1, \tag{3.28}$$

$$a_1 \neq 0. \tag{3.29}$$

The last condition is necessary for both the wavelength and the period to have the assumed value of 2π.

Evidently there is an infinite family of first-order solutions. As pointed out by Penney & Price (1952), each of these solutions will generate a different series of higher-order solutions. We follow these authors and choose to investigate only the solution that is simply periodic for small amplitudes. That is, we set $a_m = 0$ for $m > 1$; it then follows from (3.28) that $a_1 = 1$.†

For $l > 1$, we find that

$$f^{(l)} = \sum_{\mu=1}^{L(l)} \sum_{\nu=1}^{L(l)} f_{\mu,\nu}^{(l)} \sin(mt)\cos(nx), \tag{3.30}$$

$$g^{(l)} = \sum_{\mu=1}^{L(l)} \sum_{\nu=1}^{L(l)} g_{\mu,\nu}^{(l)} \sin(mt)\cos(nx), \tag{3.31}$$

$$h^{(l)} = \sum_{\mu=1}^{L(l)} \sum_{\nu=1}^{L(l)} h_{\mu,\nu}^{(l)} \cos(mt)\cos(nx), \tag{3.32}$$

where $L(l)$ is an integer function of l (to be specified later), and

$$m = 2\mu - 1, \quad n = 2\nu - 1 \quad (l \text{ odd}), \tag{3.33a, b}$$

$$m = 2\mu - 2, \quad n = 2\nu - 2 \quad (l \text{ even}) \tag{3.34a, b}$$

† In appendix A we illustrate by a simple example a possible procedure for determining higher-order solutions corresponding to other choices of a_m for $m > 1$.

The $f^{(l)}_{\mu,\nu}$, $g^{(l)}_{\mu,\nu}$ and $h^{(l)}_{\mu,\nu}$ are constants, independent of t and x. The general periodic solution of (3.7)–(3.12) may be written in the form

$$\eta^{(l)} = \sum_{\mu=1}^{L(l)} \sum_{\nu=1}^{L(l)} a^{(l)}_{\mu,\nu} \eta_{m,n}, \tag{3.35}$$

$$\phi_1^{(l)} = \sum_{\mu=1}^{L(l)} \sum_{\nu=1}^{L(l)} b^{(l)}_{\mu,\nu} \phi_{1m,n}, \tag{3.36}$$

$$\phi_2^{(l)} = \sum_{\mu=1}^{L(l)} \sum_{\nu=1}^{L(l)} c^{(l)}_{\mu,\nu} \phi_{2m,n}, \tag{3.37}$$

where m and n are defined by (3.33) or (3.34) and $a^{(l)}_{\mu,\nu}$, $b^{(l)}_{\mu,\nu}$, $c^{(l)}_{\mu,\nu}$ are independent of t and x. Substitution of (3.30)–(3.32) and (3.35)–(3.37) into (3.9), (3.10) gives

$$a^{(l)}_{\mu,\nu} = \frac{nh^{(l)}_{\mu,\nu} + mf^{(l)}_{\mu,\nu} + rmg^{(l)}_{\mu,\nu}}{S^{(0)}(n-m^2)}, \tag{3.38}$$

$$b^{(l)}_{\mu,\nu} = -\frac{f^{(l)}_{\mu,\nu} + ma^{(l)}_{\mu,\nu}}{n}, \tag{3.39}$$

$$c^{(l)}_{\mu,\nu} = \frac{g^{(l)}_{\mu,\nu} + ma^{(l)}_{\mu,\nu}}{n}, \tag{3.40}$$

for $m = 0, 1, 2, \ldots$; $n = 1, 2, 3, \ldots$; $n \neq m^2$. For $n = 0$, which implies that l is even and $\nu = 1$, the boundary conditions (3.8) and the requirement that the undisturbed interface be located along $y = 0$ give

$$a^{(l)}_{\mu,1} = b^{(l)}_{\mu,1} = c^{(l)}_{\mu,1} = 0 \quad (\mu = 1, 2, 3, \ldots). \tag{3.41}$$

Then (3.10) implies

$$B^{(l)} = \begin{cases} -\sum_{\mu=1}^{L(l)} h^{(l)}_{\mu,1} \cos(mt) & (l \text{ even}), \qquad (3.42a) \\ 0 & (l \text{ odd}). \qquad (3.42b) \end{cases}$$

For $m = n = 1$, which implies that l is odd and $\mu = \nu = 1$, (3.38) is replaced by

$$S^{(l-1)} = \begin{cases} h^{(l)}_{1,1} + f^{(l)}_{1,1} + rg^{(l)}_{1,1} & (l \text{ odd}), \qquad (3.43a) \\ 0 & (l \text{ even}). \qquad (3.43b) \end{cases}$$

This leaves $a^{(l)}_{1,1}$, for l odd, undetermined; however, (3.12) may be used to give

$$a^{(l)}_{1,1} = -\sum_{\mu=1}^{L(l)} \sum_{\nu=1}^{L(l)} a^{(l)}_{\mu,\nu} \quad (l \text{ odd}) \tag{3.44}$$

(where $a^{(l)}_{1,1}$ in the sum is set to zero) when all the other coefficients in the sum are known. The coefficients $b^{(l)}_{1,1}$ and $c^{(l)}_{1,1}$, for l odd, are then determined by (3.39) and (3.40).

The cases $n = m^2$ ($n \neq 0, 1$) are more complicated. Let μ^*, ν^* be the values of the indices corresponding to one of these cases, then (3.38) is replaced by

$$m^2 h^{(l)}_{\mu^*,\nu^*} + mf^{(l)}_{\mu^*,\nu^*} + rmg^{(l)}_{\mu^*,\nu^*} = 0, \tag{3.45}$$

and $a^{(l)}_{\mu^*,\nu^*}$ is undetermined. Indeed, the $a^{(l)}_{\mu^*,\nu^*}$ are coefficients of the homogeneous solutions to (3.9) and (3.10), as indicated by (3.23). Assume that (3.45) is satisfied at order l for $l > 2$. If $a^{(l)}_{\mu^*,\nu^*}$ is given an arbitrary value, then some careful algebra shows that at order $l+2$ (3.45) will be

$$\alpha a^{(l)}_{\mu^*,\nu^*} + \beta = 0, \tag{3.46}$$

where $$\alpha = m^2(m^2-1)\left[\frac{r}{1+r}\right] - m^2 S^{(2)}, \tag{3.47}$$

and β is a constant that is determined by computing the left-hand side of (3.45) at order $l+2$ with $a^{(l)}_{\mu^*,\nu^*} = 0$ (in general $\beta \neq 0$). Therefore an arbitrary choice of $a^{(l)}_{\mu^*,\nu^*}$ will not satisfy (3.45). But it is always possible to satisfy (3.45) at order $l+2$ by choosing

$$a_{\mu^*,\nu^*} = -\frac{\beta}{\alpha}, \tag{3.48}$$

unless, using the expression for $S^{(2)}$ given by (4.4),

$$r = 2(m^2-1) - [4(m^2-1)^2 - 1]^{\frac{1}{2}}, \tag{3.49}$$

in which case $\alpha = 0$. The values of r that satisfy (3.49) corresponding to several values of m are given in table 1. Note that as m increases, r approaches the free-surface limit $r = 0$. The air–water density ratio, $r = 10^{-3}$, lies between $m = 15$ and $m = 16$. In the present work we will not investigate the standing waves corresponding to these particular values of r, except to note, where appropriate below, how the present method may possibly be modified to handle these special cases.

With $a^{(l)}_{\mu^*,\nu^*}$ given by (3.48), the coefficients $b^{(l)}_{\mu^*,\nu^*}$ and $c^{(l)}_{\mu^*,\nu^*}$ are determined by (3.39) and (3.40). It follows from this procedure that for a general value of $0 \leqslant r \leqslant 1$, the integer function $L(l)$ is given by

$$L(l) = \begin{cases} [\frac{1}{2}l]+1 & (1 \leqslant l < 4), \qquad (3.50a) \\ [\frac{1}{2}l]+N & (3+N^2 \leqslant l < 3+(N+1)^2,\ N = 1, 2, \ldots), \qquad (3.50b) \end{cases}$$

where the symbol $[\frac{1}{2}l]$ represents the integer part of $\frac{1}{2}l$. It is interesting that (3.50) violates Stokes' hypothesis; that is, the solution (3.35)–(3.37) does not have the property that the nth-degree Fourier component first appears at nth order. For this to be true, $L(l)$ must be equal $[\frac{1}{2}l]+1$ for all l. From the results to be presented in §4 it appears that for the two special cases $r = 0, 1$ Stokes' hypothesis is correct; that is, all the coefficients in (3.35)–(3.37) with $r = 0, 1$ and indices $\mu, \nu > [\frac{1}{2}l]+1$ have been found to be zero, up to $l = 21$. We have not been able to prove that this is true for all l. Schwartz & Whitney (1981) in their solution of the free-surface standing-wave problem assumed from the beginning that the structure of the perturbation solution followed Stokes' hypothesis.

We have not derived explicit formulae for the $f^{(l)}_{\mu,\nu}$, $g^{(l)}_{\mu,\nu}$ and $h^{(l)}_{\mu,\nu}$ coefficients. Indeed, explicit formulae for these quantities would be much too complicated to express clearly because their calculation involves many multiplications of double Fourier series. Instead, we have devised an algorithm for computing the values of these coefficients. The algorithm is outlined in appendix B.

The general procedure for $l > 1$, with r not equal to one of the values given by (3.49), is as follows. Assuming that the complete solution is known for all orders less than or equal to $l-1$, compute $f^{(l)}_{\mu,\nu}$, $g^{(l)}_{\mu,\nu}$ and $h^{(l)}_{\mu,\nu}$, for $\mu, \nu = 1, 2, \ldots L(l)$, by the method described in appendix B. Next compute $a^{(l)}_{\mu,\nu}$, $b^{(l)}_{\mu,\nu}$ and $c^{(l)}_{\mu,\nu}$, for $\mu, \nu = 1, 2, \ldots L(l)$, from (3.38)–(3.41) if l is even, or from (3.38)–(3.40) and (3.44) if l is odd, setting $a^{(l)}_{\mu^*,\nu^*} = 0$ (where μ^*, ν^* are such that $n = m^2$, $n \neq 0, 1$). At the same time, compute $B^{(l)}$ from (3.42) and $S^{(l-1)}$ from (3.43). This procedure is then repeated for $l = l+1$ and $l = l+2$. At order $l+2$, compute $a^{(l+2)}_{\mu^*,\nu^*}$ from (3.48) and recompute $b^{(l+2)}_{\mu^*,\nu^*}$ and $c^{(l+2)}_{\mu^*,\nu^*}$ from (3.39) and (3.40). Finally, if l is odd, recompute $a^{(l)}_{1,1}$ from (3.44). This gives the complete solution for order l. This entire process may be continued for $l = l+1, l+2, \ldots$, etc.

m	r
2	0·083920
3	0·031281
4	0·016671
5	0·010418
⋮	⋮
15	0·001116
16	0·000980

TABLE 1. The values of the density ratio r that satisfy (3.49) for several different values of m

The general procedure for $l > 1$, with r equal to one of the values given by (3.49), should be similar to but more complicated than the procedure described above. The essential difference should be that instead of carrying the calculation forward two orders to determine the particular $a^{(l)}_{\mu^*,\nu^*}$ corresponding to the singular value of m, the calculation will have to be carried forward three or possibly four orders. Because the algebra is complicated, we have not attempted to prove that this procedure will indeed eliminate resonance at all orders.

The algorithm described above was first programmed in CAMAL, an algebraic computing language developed at Cambridge University. The highest order that could be calculated using this method was determined by storage limitations. For a fifth-order calculation, which is the highest-order calculation we made using CAMAL, the execution time was approximately one minute and the store was 250 Kbytes on the Cambridge University IBM 370/165. The solution to fourth order is shown in §4. This solution matches Hunt's (1961) fourth-order solution, except that the coefficients Hunt found to be indeterminate we have determined by requiring secularity to be eliminated at sixth order.

Although the CAMAL program is general in that it gives the solution in terms of the algebraic variable r, a solution to fifth order is not sufficient to compute the limiting-amplitude standing waves. To compute a higher-order solution we programmed the calculation in FORTRAN IV and ran the calculation in double precision (29 decimal digits) on the CDC 7600 at the Lawrence–Berkeley Laboratories in Livermore, California. A 21st-order calculation required approximately three minutes of execution time and 220 Kwords of store. We ran the FORTRAN program for five different values of the density ratio: $r = 0, 10^{-3}, 0{\cdot}1, 0{\cdot}5, 1$. The first value corresponds to free-surface waves, the second value to air–water interfacial waves, the third and fourth values correspond to intermediate density ratios, and the last value corresponds to Boussinesq waves, in which the density difference is only important when associated with buoyancy.

Several methods were used to check the accuracy of the FORTRAN program. To fifth order, the calculations were compared with the CAMAL results, and were found to agree to full machine accuracy for all values of the density ratio used. There are no higher-order interfacial standing-wave solutions available, but we did compare our $r = 0$ solution to Schwartz & Whitney's (1981) 25th-order free-surface standing-wave solution. Up to 21st-order, which is the highest order we computed, our coefficients for the expansion of S were found to agree with Schwartz & Whitney's (to the number of figures they display). Because of the different formulations, it is difficult to compare the other aspects of the two calculations. We also computed the terms in (2.16) and found that the equation was always balanced within machine accuracy.

4. Results

We use rational fractions (Padé approximants) to sum the twenty-first order series for the wave period, the wave energy and the wave profile. The $[M/N]$ Padé approximant of a function $f(\epsilon)$ that has the series expansion

$$f(\epsilon) = a_0 + a_1\epsilon + a_2\epsilon^2 + \ldots + a_{M+N}\epsilon^{M+N} + \ldots \tag{4.1}$$

is defined as

$$[M/N] = \frac{b_0 + b_1\epsilon + \ldots + b_m\epsilon^M}{1 + c_1\epsilon + \ldots + c_N\epsilon^N}, \tag{4.2}$$

where b_i and c_i are determined uniquely by equating coefficients of equal powers of ϵ between (4.1) and the Taylor-series expansion of (4.2) about $\epsilon = 0$.

Rational fractions provide an approximate method of analytic continuation. The convergence of the simple series (4.1) is confined to values of $|\epsilon|$ less than $|\epsilon^*|$, where ϵ^* is the location in the complex plane of the singularity of f that is nearest the origin. The sequence of Padé approximants (4.2), on the other hand, will usually only fail to converge near branch points or branch cuts of f. Padé approximants are known to have poles near the singularities of f. By our definition (3.6), only real values of ϵ are physically meaningful. Thus the position of the pole that is on the real axis and nearest the origin gives an indication of the maximum value of ϵ for which physically meaningful solutions exist.

Padé approximants have been used with much success in water-wave theory by Schwartz (1974), Longuet-Higgins (1975), Cokelet (1977), Holyer (1979), Schwartz & Whitney (1981), and others. Baker (1965), Graves-Morris (1973) and Cabannes (1976) may be consulted for the theory and applications of Padé approximants.

4.1. *The wave period*

The dimensional wave period T' is related to our non-dimensional parameter S by

$$T'^2 = \frac{2\pi\lambda}{g(1-r)}S. \tag{4.3}$$

To fourth order, the coefficients in the expansion of S for $0 \leqslant r \leqslant 1$ are

$$S^{(0)} = 1 + r, \tag{4.4a}$$

$$S^{(2)} = -\tfrac{1}{4}(1-r) + \tfrac{1}{2}q, \tag{4.4b}$$

$$S^{(4)} = \frac{1}{4}\left(\frac{39}{32} - \frac{5}{32}r - 3q + \frac{13}{4}q^2 - \frac{13}{8}q^3\right), \tag{4.4c}$$

where

$$q \equiv (1+r)^{-1}. \tag{4.5}$$

As mentioned before, all coefficients of the odd powers of ϵ in the series for S are zero. To 21st order, the coefficients in the expansion for S for the five values of the density ratio considered are shown in table 2.

The locations of the poles of the $[N/N]$ and $[N/N+1]$ Padé approximants to S on the real axis and nearest the origin for each of the five cases considered are presented in table 3. Although we clearly have an insufficient number of terms to give a conclusive answer, the results are fairly consistent except for $r = 0{\cdot}1$. The average of the last three approximants gives $\epsilon_{\max} \equiv 0{\cdot}68, 0{\cdot}68, 2{\cdot}48, 0{\cdot}93, 1{\cdot}03$ for $r = 0, 10^{-3}, 0{\cdot}1, 0{\cdot}5, 1{\cdot}0$ respectively.

The summed Padé approximants for S as a function of ϵ are plotted in figure 2. These curves were obtained by computing the average of the [3/4], [4/4], [4/5] and

l	$r = 0$	$r = 10^{-3}$	$r = 0{\cdot}1$	$r = 0{\cdot}5$	$r = 1{\cdot}0$
0	1·0	1·001	1·1	1·5	2·0
2	0·250000	0·249751	0·229546	0·208333	0·250000
4	−0·039063	−0·038759	−0·014771	0·025897	0·042969
6	−0·015431	−0·015020	0·018699	0·013429	0·010274
8	−0·010839	−0·010500	−0·059273	0·002469	0·009469
10	−0·063683	−0·062969	0·446949	0·008036	·0·006971
12	−0·134050	−0·132736	−3·257306	0·006631	0·007264
14	−0·238688	−0·237784	23·55961	0·019791	0·004842
16	−0·532647	−0·532529	−170·2927	0·091857	0·010320
18	−1·242121	−1·243090	1233·421	0·650268	−0·075973
20	−2·724052	−2·733988	−8946·606	6·493484	−0·766586

TABLE 2. Coefficients of ϵ^l in the series expansion of S for several values of the density ratio r

$[M/N]$	$r = 0$	$r = 10^{-3}$	$r = 0{\cdot}1$	$r = 0{\cdot}5$	$r = 1{\cdot}0$
[2/2]	1·224532	1·228945	—	1·902278	0·632469
[2/3]	0·435644	0·431892	3·061098	1·025025	1·026655
[3/3]	0·629205	0·627329	1·583332	0·881641	1·034779
[3/4]	0·744248	0·741132	2·777643	1·108724	1·025469
[4/4]	0·688748	0·687293	2·865091	0·935272	1·048303
[4/5]	0·675703	0·674576	2·777681	0·910924	1·020545
[5/5]	0·674083	0·673078	1·803355	0·935718	1·043851

TABLE 3. Positions of the poles of the $[N/N]$ and $[N/N+1]$ approximants of S that are located on the real axis and nearest the origin

[5/5] Padé approximants for a given value of ϵ, discarding the approximant that was furthest from the mean, plotting the new average of the remaining three approximants as a solid line, and plotting the deviation from the mean as dashed lines on either side of the solid curve. The figure shows that S increases monotonically with increasing ϵ for all five values of r, although there is a hint that S is maximum for some $\epsilon < \bar{\epsilon}_{\max}$ when $r = 0$.

4.2. *The wave energy*

The total energy per unit horizontal area is, since the motion comes completely to rest at $t = n\pi$, $n = 0, 1, \ldots$, simply the potential energy per unit horizontal area evaluated at $t = 0$. In terms of dimensional quantities, the potential energy per unit horizontal area of the two-fluid system is

$$V(t) = \frac{1}{\lambda}\int_0^{\lambda}\int_0^{\eta(x)} (\rho_1 - \rho_2)\, g y \, dy \, dx. \tag{4.6}$$

If we let

$$\tilde{V} = \frac{k^2}{(\rho_1 - \rho_2)\, g} V, \tag{4.7}$$

where the tilde denotes a non-dimensional variable, then in non-dimensional form, dropping the tildes, (4.6) is

$$V(t) = \tfrac{1}{2}\overline{\eta^2}, \tag{4.8}$$

where the overbar denotes horizontal average over one wavelength.

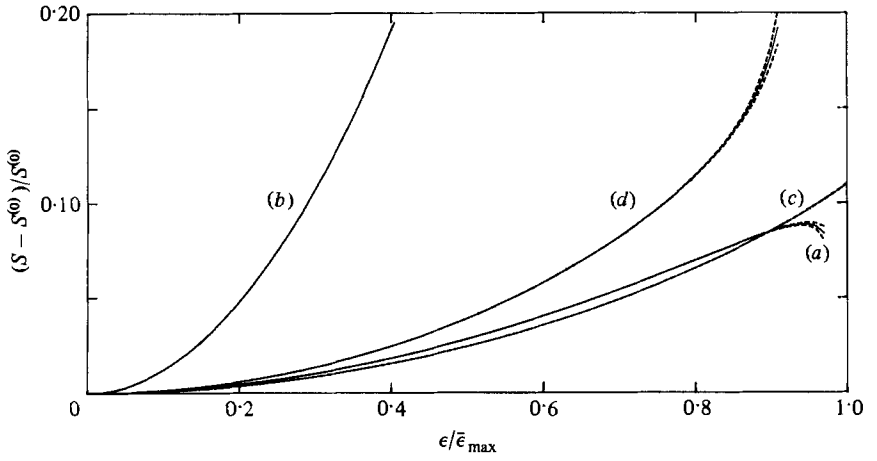

FIGURE 2. The increase of S, which is proportional to the square of the wave period, relative to the value of S for infinitesimal waves, as a function of the expansion parameter ϵ. The solid curves are the average of three Padé approximants and the dashed curves indicate the deviation from this average. $\bar{\epsilon}_{\max} = 0{\cdot}68,\ 2{\cdot}41,\ 0{\cdot}83,\ 1{\cdot}09$ for $r = (a)\ 0,\ (b)\ 0{\cdot}1,\ (c)\ 0{\cdot}5,\ (d)\ 1{\cdot}0$.

To fourth order, the series expansion of E, the total energy per unit horizontal area, is

$$E = \sum_{l=0}^{\infty} E^{(l)}\epsilon^l, \tag{4.9}$$

where
$$E^{(0)} = 0, \quad E^{(2)} = \tfrac{1}{4}, \quad E^{(4)} = -\tfrac{1}{8}+\tfrac{3}{4}q-\tfrac{3}{4}q^2, \tag{4.10a, b, c}$$

and all $E^{(l)}$ for odd l are zero. To 21st order, the coefficients in the expansion for E are shown in table 4. The locations of the limiting poles of the $[N/N]$ and $[N/N+1]$ approximants to E for each of the five density ratios considered are presented in table 5. The average of the last three approximants gives $\epsilon_{\max} = 0{\cdot}68,\ 0{\cdot}68,\ 2{\cdot}33,\ 0{\cdot}73,\ 1{\cdot}15$ for $r = 0,\ 10^{-3},\ 0{\cdot}1,\ 0{\cdot}5,\ 1{\cdot}0$ respectively.

The summed Padé approximants for E as a function of ϵ are plotted in figure 3. These curves are computed by the method described in §4.1. The figure shows that E increases monotonically with increasing ϵ for all five values of r, although there is a hint that E is maximum for some $\epsilon < \bar{\epsilon}_{\max}$ when $r = 0$.

4.3. *The wave profile*

The fourth-order expansion for the interface profile is conveniently written in the form

$$\eta(t, x) = A_1\cos x + A_2\cos 2x + A_3\cos 3x + A_4\cos 4x, \tag{4.11}$$

where

$$A_1 = \epsilon\cos t - \tfrac{1}{16}\epsilon^3[(5-29q+29q^2)\cos t + (1-3q+3q^2)\cos 3t], \tag{4.12a}$$

$$A_2 = -\epsilon^2(\tfrac{1}{4}-\tfrac{1}{2}q)(1+\cos 2t) + \epsilon^4[\tfrac{1}{16}(\tfrac{9}{4}-21q+\tfrac{99}{2}q^2-33q^3)+(\tfrac{1}{3}-\tfrac{13}{6}q+\tfrac{9}{2}q^2-3q^3)\cos 2t + \tfrac{1}{112}(\tfrac{67}{12}-\tfrac{95}{3}q+\tfrac{123}{2}q^2-41q^3)\cos 4t], \tag{4.12b}$$

$$A_3 = \epsilon^3[(\tfrac{3}{16}-q+q^2)(\tfrac{3}{2}\cos t+\tfrac{1}{2}\cos 3t)], \tag{4.12c}$$

$$A_4 = -\epsilon^4[(\tfrac{1}{8}-\tfrac{5}{4}q+3q^2-2q^3)(1+\tfrac{1}{3}\cos 4t)-b\cos 2t]; \tag{4.12d}$$

$$b = [14(1-q)-(1+r)]^{-1}(\tfrac{927}{224}-\tfrac{3}{16}r-\tfrac{20933}{672}q+\tfrac{28591}{336}q^2-\tfrac{8105}{84}q^3+\tfrac{1621}{42}q^4) \tag{4.13}$$

l	$r = 0$	$r = 10^{-3}$	$r = 0{\cdot}10$	$r = 0{\cdot}5$	$r = 1{\cdot}0$
2	0·250000	0·250000	0·250000	0·250000	0·250000
4	−0·125000	−0·124252	−0·063017	0·041667	0·062500
6	0·090503	0·090123	0·071168	0·016925	0·008049
8	−0·025652	−0·025518	−0·087564	−0·001786	0·004940
10	−0·126169	−0·124514	0·509042	0·007742	0·003165
12	−0·064908	−0·064235	−3·743508	0·004748	0·003169
14	−0·174268	−0·175055	27·17559	0·021102	0·000367
16	−0·546307	−0·545659	−196·4122	0·106552	0·004496
18	−1·127015	−1·127782	1421·833	0·776879	−0·082328
20	−2·346874	−2·361131	−10307·94	7·806961	−0·789108

TABLE 4. Coefficients of ϵ^l in the series expansion of E for several values of the density ratio r

$[M/N]$	$r = 0$	$r = 10^{-3}$	$r = 0{\cdot}1$	$r = 0{\cdot}5$	$r = 1{\cdot}0$
[2/2]	—	—	—	1·885219	1·249028
[2/3]	—	—	1·597955	0·629427	1·000640
[3/3]	0·736978	0·734699	—	0·650101	1·173273
[3/4]	0·682305	0·680800	2·637897	0·630756	1·175324
[4/4]	0·670844	0·669960	—	0·863524	1·173271
[4/5]	0·674487	0·673438	2·020076	0·683986	1·088318

TABLE 5. Position of the poles of the $[N/N]$ and $[N/N+1]$ approximants of E that are located on the real axis and nearest the origin

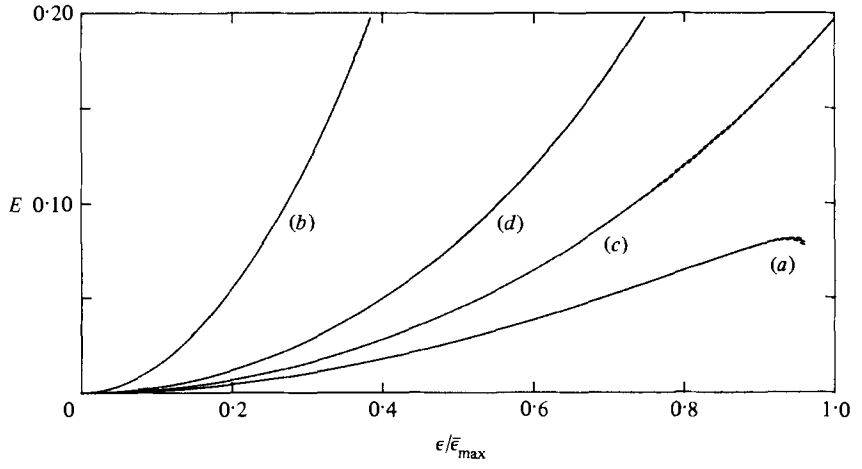

FIGURE 3. The wave energy E plotted against the expansion parameter ϵ. The solid curves are the average of three Padé approximants and the dashed curves indicate the deviation from this average. $\bar{\epsilon}_{max}$ = 0·68, 2·41, 0·83, 1·09 for r = (*a*) 0, (*b*) 0·1, (*c*) 0·5, (*d*) 1·0.

for $$r \neq 6 - \sqrt{35}. \tag{4.14}$$

If the differences in the definition of the expansion parameter and the phase of the generating solution are taken into account, the above solution agrees with the solution given by Hunt (1961, equation (19)). However, Hunt found the coefficient b to be indeterminate, whereas we have found that the value shown above for this coefficient is necessary to eliminate secularity at sixth order.

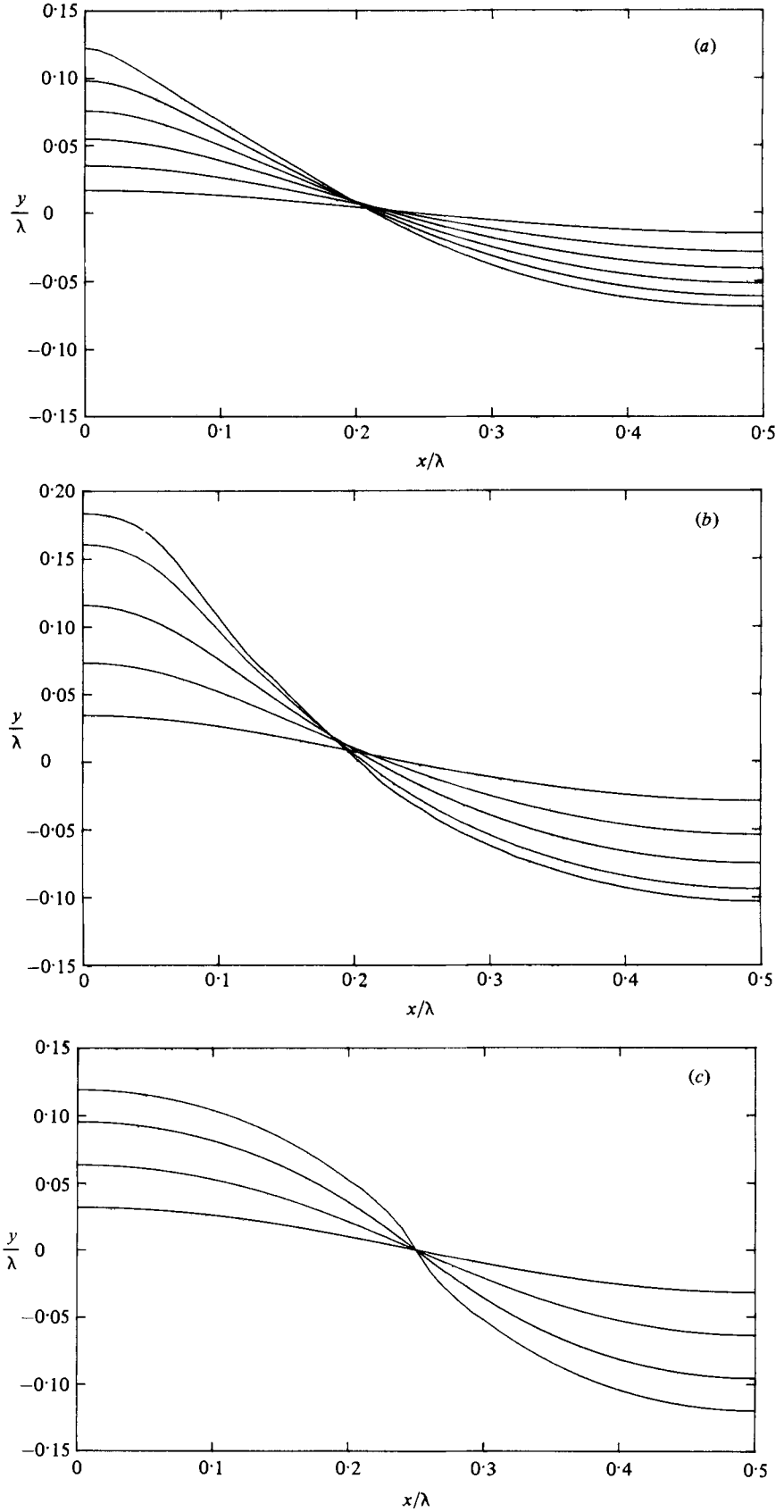

FIGURE 4. For caption see facing page.

The results of the 21st-order calculation for the three cases $r = 0, 0{\cdot}1, 1{\cdot}0$ are shown in figures 4(*a–c*) and figures 5(*a–c*). The plots in figure 4 were obtained by using the method described in §4.1 to sum the series for $\eta(t, x)$ at 100 values of x equally spaced between 0 and π for $t = 0$, and connecting all the computed points with straight lines. Different wave amplitudes for each density ratio are shown in figures 4(*a–c*). The highest wave in each plot is the largest-amplitude wave for which Padé approximants produce visibly smooth curves. All the other waves plotted in these figures are computed from Padé approximants that have converged to within one percent or better.

The plots in figure 5 show the interface for one wave height at 9 equally spaced times between 0 and π (a half-cycle). The interface, shown as a solid curve, was computed as in figure 4. The positions of the lower fluid particles, represented by solid circles, and of the upper fluid particles, represented by solid squares, were computed by numerically integrating the equations

$$\frac{dX}{dt} = \frac{\partial \phi}{\partial x}\bigg|_{(x,y)=(X,Y)}, \quad \frac{dY}{dt} = \frac{\partial \phi}{\partial y}\bigg|_{(x,y)=(X,Y)}, \tag{4.15a, b}$$

where $(X(t), Y(t))$ is the particle position at time t. In the numerical integration the right-hand sides of (4.15a, b) were computed from the 21st-order series for ϕ by the method described in §4.1. The particle trajectories are shown as dotted lines in the figures.

There are several conclusions to be drawn from these two sets of graphs. Both sets of curves show that as the density ratio approaches unity, the interface profile becomes more sinusoidal than the free-surface profile. That is, the presence of an upper fluid tends to reduce the magnitude of the coefficients of the higher harmonics in the solution for the interface profile. In fact, it is not difficult to show that Boussinesq ($r = 1$) standing waves have the additional symmetry $\eta(x) = -\eta(x+\pi)$ as well as the assumed symmetry $\eta(x) = -\eta(-x)$. From a physical point of view, the closer the density ratio is to unity, the lesser the effect of gravity is, and thus the difference between crests and troughs is less, until at $r = 1$ crests and troughs are identical in shape. In other words, with no preferred direction in the vertical, the wave should look the same viewed from below as from above.

The profiles illustrated in figures 4(*a–c*) show that as the amplitude of the waves nears its maximum, the slope at some point along the profile appears to approach the vertical, except for the free-surface standing waves. For free-surface waves, the slope at the crest appears to be approaching 45°, although we do not have sufficient accuracy with only 21 terms in our expansion to say this for certain. As r increases from 0 to 1 the point on the interface with vertical slope moves from very near the crest to the midpoint between the crest and the trough. This is exactly the same behaviour exhibited by near-maximum amplitude interfacial progressive waves, as described by Holyer (1979). However, for standing waves we do not have sufficient accuracy to determine the exact position along the interface where the profile becomes vertical for each density-ratio case, as Holyer (1979) was able to do for progressive waves using a 31-term expansion.

Figure 5(*a*) shows, as pointed out by Penney & Price (1952) and Schwartz & Whitney (1981), that free-surface waves are never flat. They are most nearly flat at

FIGURE 4. Interface profiles at $t = 0$ for several amplitudes of oscillation: (*a*) free-surface waves, $\rho_2/\rho_1 = 0$ at $\epsilon = 0{\cdot}1, 0{\cdot}3, 0{\cdot}4, 0{\cdot}5, 0{\cdot}5, 0{\cdot}6$; (*b*) interfacial waves, $\rho_2/\rho_1 = 0{\cdot}1$ at $\epsilon = 0{\cdot}2, 0{\cdot}4, 0{\cdot}6, 0{\cdot}8, 0{\cdot}9$; (*c*) Boussinesq waves, $\rho_2/\rho_1 = 1{\cdot}0$ at $\epsilon = 0{\cdot}2, 0{\cdot}4, 0{\cdot}6, 0{\cdot}75$.

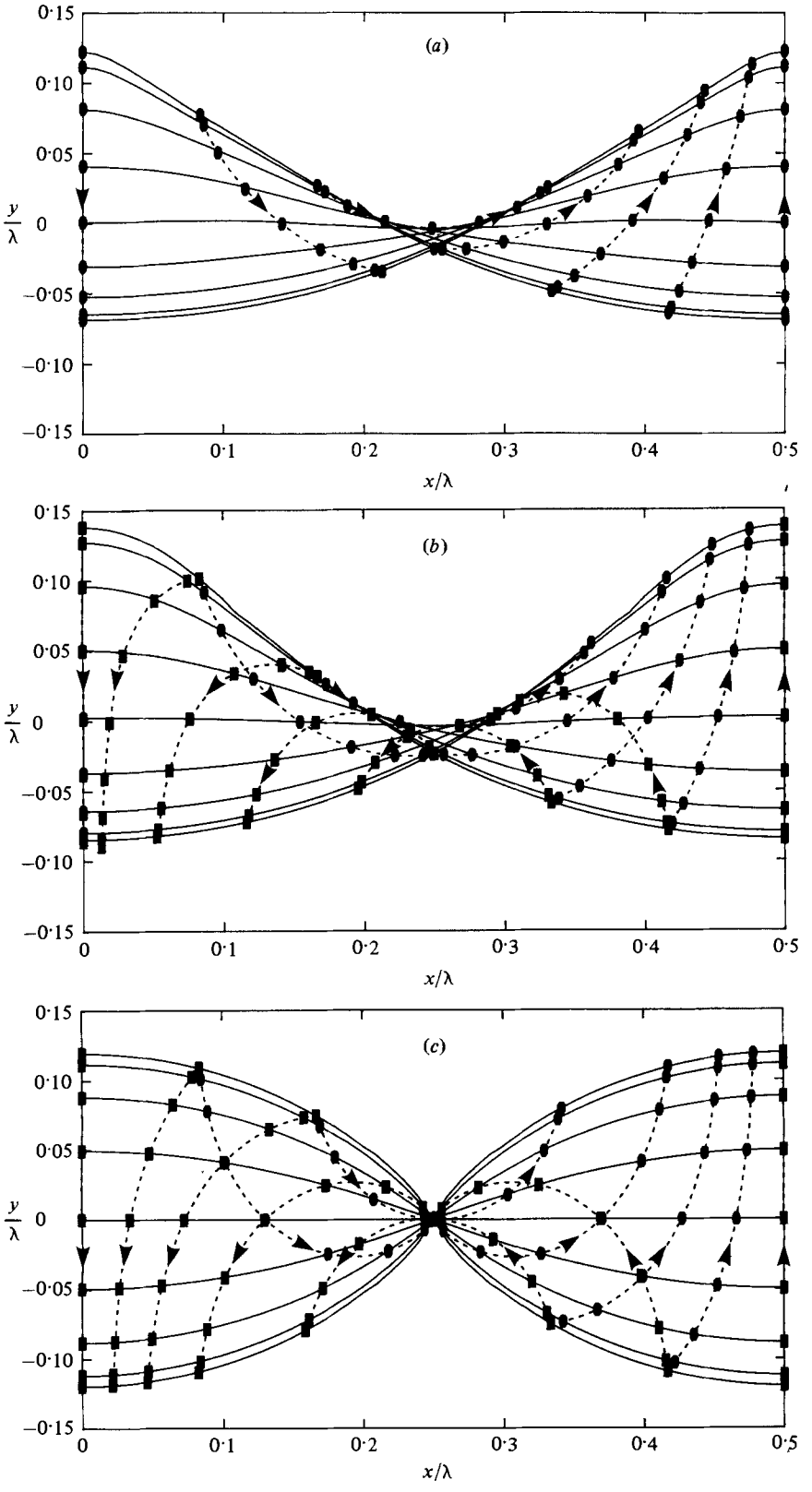

FIGURE 5. For caption see facing page.

$t = \frac{1}{2}\pi \pm n\pi$, $n = 1, 2, \ldots$. Figure 5 (*c*) illustrates that, contrary to free-surface standing waves, interfacial waves are flat at $t = \frac{1}{2}\pi \pm n\pi$. This can be inferred from the symmetry relation $\eta(t, x) = -\eta(t, x+\pi)$, which requires that $\eta(t, x)$ has a Fourier expansion in terms of cosine functions with arguments that are odd integer multiples of t and x.

4.4. *Discussion of the highest wave*

We have used the locations of the poles of the Padé approximants to the wave period and the wave energy to estimate the maximum height that standing waves can achieve before they become non-periodic. Averaging the estimates obtained from the two series we get: $\bar{\epsilon}_{\max} = 0{\cdot}68$, $0{\cdot}68$, $2{\cdot}41$, $0{\cdot}83$, $1{\cdot}09$ for $r = 0$, 10^{-3}, $0{\cdot}1$, $0{\cdot}5$, $1{\cdot}0$ respectively. Comparing the results from the two series, we find good agreement for $r = 0$, 10^{-3}, but discrepancies as high as 20 % for $r = 0{\cdot}1, 0{\cdot}5, 1{\cdot}0$. Thus, our estimates for the maximum wave height for $r > 0$ must be considered uncertain. However, the trends are consistent; interfacial waves tend to have a larger maximum amplitude than free-surface waves, and waves with $r \approx 0{\cdot}1$ tend to have a much larger maximum amplitude than either free-surface or Boussinesq waves.

By analogy with progressive waves, we would expect the maximum amplitude to increase monotonically with increasing r. Our results for $r = 0{\cdot}1$ are inconsistent with this expectation. Since we have been unable to determine a physical reason for the predicted large maximum amplitude for this case, we feel that the nearness of $r = 0{\cdot}1$ to $0{\cdot}083\,92\ldots$, the largest value of r for which the solution procedure fails, affects the accuracy of our results. Therefore, our results for this case must be considered very uncertain.

The apparent maximum in S and E for $\epsilon < \epsilon_{\max}$ when $r = 0$ can be explained just as for progressive waves. At $t = 0$ the highest wave is sharp-crested, and its profile intersects that of slightly smaller amplitude waves near the crest, which means that the highest wave is actually lower over most of the profile.

As a check on our procedure for estimating the maximum wave height, we computed Padé approximants to the vertical pressure gradient at the crest of free-surface standing waves at $t = 0$. In non-dimensional form, the vertical pressure gradient is given by

$$\frac{\partial p}{\partial y} = -\left(\frac{\partial^2 \eta}{\partial t^2} + S\right). \tag{4.16}$$

The results for the [8/8], [9/9] and [10/10] approximants are plotted in figure 6. According to Penney & Price (1952), the free-surface standing wave of maximum height has a downward acceleration at the crest equal to that due to gravity, which implies that the right-hand side of (4.16) is zero. In figure 6, the Padé approximants for the right-hand side of (4.16) are seen to cross zero at $\epsilon_{\max} \approx 0{\cdot}647$, which gives $(H/\lambda)_{\max} \approx 0{\cdot}206$. This is very close to our previous estimate of $\epsilon_{\max} \approx 0{\cdot}68$.

As another check on our calculation of free-surface standing waves of maximum height, we computed γ, the initial inclination of surface particle trajectories to the downward vertical. The results near the crest for $\epsilon = 0{\cdot}3$, $0{\cdot}4$ and $0{\cdot}5$ are shown in figure 7. Longuet-Higgins (1973), with the assumption that the crest of the highest

---

FIGURE 5. Interface profiles (solid curves) and particle trajectories (dashed curves) at $t = 0, \frac{1}{8}\pi, \frac{2}{8}\pi, \ldots, \pi$; ●, lower fluid particles; ■, upper fluid particles. (*a*) Free-surface waves, $\rho_2/\rho_1 = 0$ at $\epsilon = 0{\cdot}6$; (*b*) interfacial waves, $\rho_2/\rho_1 = 0{\cdot}1$ at $\epsilon = 0{\cdot}7$; (*c*) Boussinesq waves, $\rho_2/\rho_1 = 1{\cdot}0$ at $\epsilon = 0{\cdot}75$.

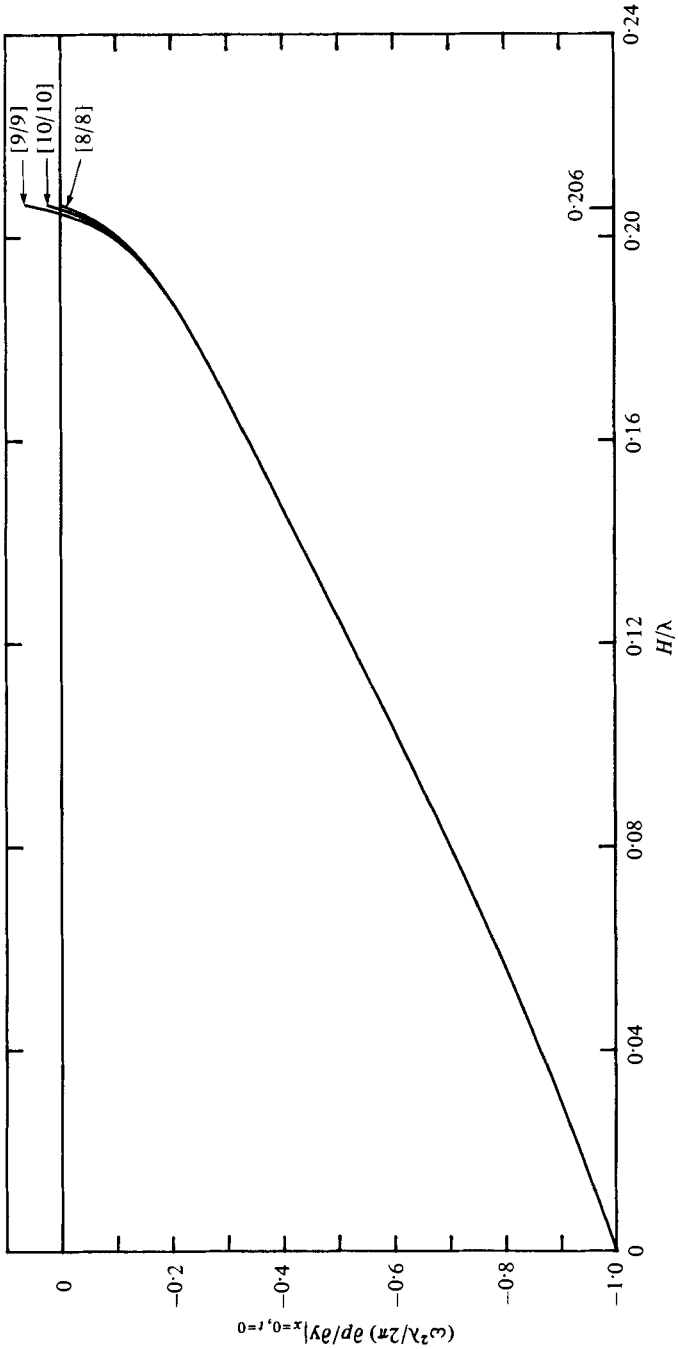

FIGURE 6. The summed [8/8], [9/9] and [10/10] Padé approximants for the vertical pressure gradient at the crest at $t = 0$ plotted against the wave height to wavelength ratio for $r = 0$. The [10/10] approximant is zero at $H/\lambda \approx 0{\cdot}206$.

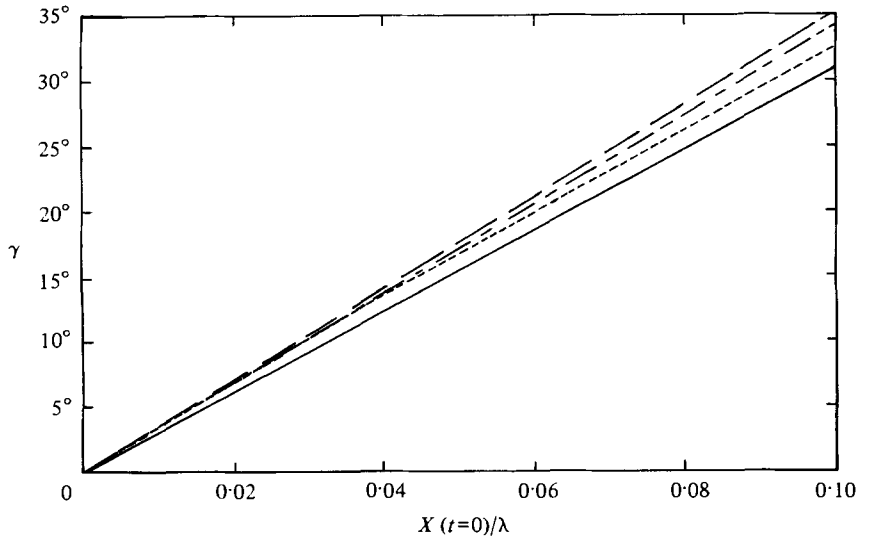

FIGURE 7. The initial inclination γ of free-surface particle trajectories to the downward vertical as a function of the initial, horizontal particle position $X(t = 0)$: ———, $\epsilon = 0{\cdot}3$; – – –, $\epsilon = 0{\cdot}4$; – – – – –, $\epsilon = 0{\cdot}5$; ——, (4.17).

standing wave encloses an angle of 90°, derived an approximate expression for the velocity field of the highest wave, which near the crest gives

$$\gamma \approx \frac{5{\cdot}38X(t=0)}{\lambda}. \tag{4.17}$$

Figure 7 indicates that our computed results approach (4.17) as ϵ increases to about $\epsilon = 0{\cdot}5$. For $\epsilon > 0{\cdot}5$, our computed results oscillate about (4.17), which we believe indicates truncation error.

Our computed interface profiles indicate that the standing wave of maximum height has a vertical slope at some point on the interface, implying that standing waves break by overturning. But the experiments by Thorpe (1968) show that Boussinesq standing waves become unstable and begin to break at amplitude less than half the amplitude at which we predict overturning. We conclude that interfacial wave breaking occurs owing to shear instability, as Thorpe suggested, and not to overturning.

5. Concluding remarks

We have formulated an algorithm for computing a series solution for the shape of the interface profile, the velocity potentials, and the period of interfacial standing waves as a function of wave amplitude. The algorithm has been coded for automatic computation using two different programming languages. Using CAMAL, a symbolic algebra language, a solution has been obtained to fifth order in terms of the algebraic variable r, the ratio of the density of the upper fluid to that of the lower fluid. Using FORTRAN, solutions have been obtained to 21st order for the five specific values of $r = 0$, 10^{-3}, $0{\cdot}1$, $0{\cdot}5$, $1{\cdot}0$.

Several features of the interfacial standing-wave problem complicate the solution algorithm. The major computational difficulty is that the boundary condition at the interface must be expanded in a Taylor series about the undisturbed interface. Unlike free-surface boundary conditions, which have constant pressure at the surface and therefore can be simplified by mapping the surface to a known, fixed region, interfacial boundary conditions cannot be so simplified. A feature that free-surface and interfacial waves have in common is that the solution to the first-order equations is not unique. For simplicity, we have followed previous workers in arbitrarily choosing the first-order solution that is simply periodic in space and time. However, the existence of these other first-order solutions leads to secularity at higher order. For this secularity to be eliminated, which is essential for the existence of periodic standing waves, we must add to the particular solutions appropriate homogeneous solutions with coefficients computed such that the secularities at higher order are eliminated. We have shown that this is always possible, except for a denumerably infinite set of values of r clustered near $r = 0$. (A procedure somewhat different from ours would have to be used at these particular values of r.) As a result of this procedure, we find that in general the structure of the solution does not conform with Stokes' hypothesis. That is, for a general value of r the solution does not have the property that the nth-degree Fourier component first appears at nth order. For two specific values of r, corresponding to free-surface waves and Boussinesq waves, the solutions do seem to have a Stokes-type expansion.

The results of the calculations show the effects of the presence of an upper fluid. In general, interfacial waves tend to have flatter crests and troughs, and longer periods than free-surface waves with the same amplitudes. The property of free-surface standing waves that the surface is never flat (and thus free-surface standing waves have no true nodes) is diminished by the presence of an upper fluid; in the limit as the density of the upper fluid approaches that of the lower fluid, the interface is flat every quarter period and has a node at the midpoint between the crest and the trough.

Based on the computed solutions, we have made some conjectures of the limiting form and some estimates of the maximum amplitude of interfacial standing waves. The computed profiles indicate that the waves are limited by the interface becoming vertical at some point. The point where this occurs moves from very close to the crest for small values of the density ratio to the midpoint between the crest and the trough for Boussinesq waves. Thus we conjecture that the criterion that limits the wave height for interfacial standing waves is the same as Holyer (1979) found for interfacial progressive waves. We have estimated the limiting wave height by studying the convergence properties of the series representations of the period and the energy of standing waves. Our estimated maximum wave-height-to-wavelength ratios are $(H/\lambda)_{\max} = 0{\cdot}21,\ 0{\cdot}21,\ 0{\cdot}76,\ 0{\cdot}26,\ 0{\cdot}35$ for $r = 0{\cdot}0,\ 10^{-3},\ 0{\cdot}1,\ 0{\cdot}5,\ 1{\cdot}0$ respectively. These are crude estimates, since we cannot compute a sufficient number of terms to produce consistent results using different estimation techniques. The estimate for the case with $r = 0{\cdot}1$ is particularly suspect, since r is near $0{\cdot}08392\ldots$, where our solution procedure is invalid. Comparisons with the experiments of Thorpe (1968) indicate that Boussinesq standing waves break at much lower amplitudes than our estimated maximum amplitudes, and therefore breaking is probably due to shear instability rather than overturning.

The author is grateful to H. E. Huppert and A. J. Roberts for several helpful discussions. Financial support was provided by the National Environment Research Council.

Appendix A. Alternative solutions

The general solution to the first-order equations is given by (3.23)–(3.27), subject to the constraints (3.28) and (3.29). In the preceeding, we assumed that $a_m = 0$ for $m \neq 1$, and showed that this assumption indeed generated solutions to the equations. We will now demonstrate by a simple example that other choices for the values of the a_m also may generate solutions; however, the a_m are not arbitrary, because only particular choices for the values of the a_m will prevent resonance from occurring at higher order.

Consider the following solution to the first-order equations for free-surface standing waves (i.e. the solution corresponding to $a_m = 0$, $m > 2$):

$$\eta^{(1)} = \eta_{1,1} + a_2 \eta_{2,4}, \tag{A 1}$$

$$\phi^{(1)} = -\phi_{1,1} - \tfrac{1}{2} a_2 \phi_{2,4}, \tag{A 2}$$

$$B^{(1)} = 0, \tag{A 3}$$

$$S^{(0)} = 1, \tag{A 4}$$

in which a_2 is arbitrary. Substitution of these formulae into (3.7)–(3.12) shows that to second order no resonance is generated, and therefore a_2 is left undetermined.

But at third order, (3.43) requires

$$S^{(2)} = \tfrac{1}{4}, \tag{A 5}$$

and (3.45) for $m = 2$ requires $\quad 16a_2^3 - S^{(2)} a_2 = 0, \tag{A 6}$

which has the solutions $\quad a_2 = 0, \pm\tfrac{1}{8}. \tag{A 7}$

The solution corresponding to $a_2 = 0$ is the one we have developed in the preceding sections. The other values of a_2 are new solutions.† We have computed the solution for this case to second order, successfully eliminating resonance at fourth order. However, we have been unable, mainly because of the complicated algebra, to prove that resonance can be eliminated at all orders, although conceivably this is possible.

These results only apply to the case $r = 0$. We can prove that no solution exists if $a_2 \neq 0$, $a_m = 0$, $m > 2$, when $r \neq 0$.

Appendix B. The algorithm for computing $f^{(l)}_{\mu,\nu}$, $g^{(l)}_{\mu,\nu}$, $h^{(l)}_{\mu,\nu}$

The functions $f^{(l)}$, $g^{(l)}$ and $h^{(l)}$ are defined by (3.13)–(3.15). Their expansions in terms of double Fourier series are given by (3.30)–(3.32). If the solution is known to order $l-1$, then the coefficients $f^{(l)}_{\mu,\nu}$, $g^{(l)}_{\mu,\nu}$ and $h^{(l)}_{\mu,\nu}$ may be obtained by equating coefficients of trigonometric terms in (3.13)–(3.15).

The computation of the right-hand sides of (3.13)–(3.15) involves the addition and multiplication of double Fourier series. The addition is straightforward. The multiplication is accomplished using an algorithm we will now outline (avoiding some details). Consider two Fourier series each consisting of sums over m and n of terms like

$$a_{m,n} \left\{ \begin{matrix} \cos \\ \sin \end{matrix} \right\} (mt) \left\{ \begin{matrix} \cos \\ \sin \end{matrix} \right\} (nx). \tag{B 1}$$

The product of two terms like (B 1) produces four trigonometric terms, consisting of all the possible combinations of the sums and differences of the two ms and the two ns, with the same coefficient. The series that represents the product is computed by adding together the coefficients of the trigonometric terms of equal argument that result from the products of the elements of the two series.

† This contradicts a statement made by Schwartz & Whitney (1981, p. 168).

REFERENCES

BAKER, G. A. 1965 The theory and application of the Padé approximant method. In *Advances in Theoretical Physics* (ed. K. Brueckner), vol. 1, pp. 1–58. Acacemic.

CABANNES, H. (ed.) 1976 *Padé Approximants Method and its Application to Mechanics.* Lecture Notes in Physics, vol. 47. Springer.

CHABERT-D'HIERES, G. 1960 Etude du clapotis. *Houille Blanche* **15**, 153–163.

COKELET, E. D. 1977 Steep gravity waves in water of arbitrary uniform depth. *Phil. Trans. R. Soc. Lond.* A **286**, 183–230.

EDGE, R. D. & WALTERS, G. 1964 The period of standing gravity waves of largest amplitude on water. *J. Geophys. Res.* **69**, 1674–1675.

FULTZ, D. 1962 An experimental note on finite-amplitude standing gravity waves. *J. Fluid Mech.* **13**, 193–212.

GRAVES-MORRIS, P. R. 1973 *Padé Approximants and their Applications.* Academic.

HOLYER, J. Y. 1979 Large amplitude progressive interfacial waves. *J. Fluid Mech.* **93**, 433–448.

HUNT, J. N. 1961 Interfacial waves of finite amplitude. *Houille Blanche* **16**, 515–531.

LONGUET-HIGGINS, M. S. 1973 On the form of the highest progressive and standing waves in deep water. *Proc. R. Soc. Lond.* A **331**, 445–456.

LONGUET-HIGGINS, M. S. 1975 Integral properties of periodic gravity waves of finite amplitude. *Proc. R. Soc. Lond.* A **342**, 157–174.

PENNEY, W. G. & PRICE, A. T. 1952 Some gravity wave problems in the motion of perfect liquids. Part II. Finite periodic stationary gravity waves in a perfect liquid. *Phil. Trans. R. Soc. Lond.* A **244**, 251–284.

RAYLEIGH, J. W. S. 1915 Deep water waves, progressive or stationary, to the third order of approximation. *Proc. R. Soc. Lond.* A **91**, 345–353.

SAFFMAN, P. G. & YUEN, H. C. 1979 A note on numerical computations of large amplitude standing waves. *J. Fluid Mech.* **95**, 707–715.

SCHWARTZ, L. W. 1974 Computer extension and analytic continuation of Stokes' expansion for gravity waves. *J. Fluid Mech.* **62**, 553–578.

SCHWARTZ, L. W. & WHITNEY, A. K. 1977 A high order series solution for standing water waves. *6th Australasian Hydraul. and Fluid Mech. Conf., Preprints of Papers Part I*, pp. 356–359.

SCHWARTZ, L. W. & WHITNEY, A. K. 1981 A semianalytic solution for nonlinear standing waves in deep water. *J. Fluid Mech.* **107**, 147–171.

SEKERZH-ZENKOVICH, YA. I. 1947 On the theory of standing waves of finite amplitude on the surface of a heavy fluid (in Russian). *Dokl. Akad. Nauk SSSR* **58**, 551–553.

SEKERZH-ZENKOVICH, YA. I. 1951 On the theory of standing waves of finite amplitude on the surface of a heavy fluid of finite depth (in Russian). *Izv. Akad. Nauk SSSR, Ser. Geogra. Geofiz.* **15**, 57–73.

SEKERZH-ZENKOVICH, YA. I. 1961 Free finite oscillations of the surface of separation of two unbounded heavy fluids of different densities, (in Russian). *Trudy Morsk. Gidrofiz. Inst.* **23**, 3–43.

TADJBAKSH, I. & KELLER, J. B. 1960 Standing surface waves of finite amplitude. *J. Fluid Mech.* **8**, 442–451.

TAYLOR, G. I. 1953 An experimental study of standing waves. *Proc. R. Soc. Lond.* A **218**, 44–59.

THORPE, S. A. 1968 On standing internal gravity waves of finite amplitude. *J. Fluid Mech.* **32**, 489–528.

WHITNEY, A. K. 1971 The numerical solution of unsteady free surface flows by conformal mapping. In *Proc. 2nd Int. Conf. Numerical Methods in Fluid Dynamics* (ed. M. Holt). Lecture Notes in Physics, vol. 8, pp. 458–462. Springer.